FARADAY:
Journal of Fundamental Physics, Research, and Applied Science
Vol. 2, No. 1, January 2026, pp. 24–33, e-ISSN: 3109-1318

Optical Band Gap of PMMA: Cody, ASF, and DASF Methods Compared to Tauc

Allif Rosyidy Hilmi[1], Yofinda Eka Setiawan[1], Nailul Hasan[1]

[1] Department of Physics, Universitas Pembangunan Nasional "Veteran" Jawa Timur, Surabaya, Indonesia, 60294.

Article Info

Article History:

Received 01 12, 2026
Revised 02 09, 2026
Accepted 02 12, 2026
Published 02 14, 2026

Keywords:

PMMA
Optical Band Gap
Tauc Method
Cody Method
ASF Method
DASF Method

Corresponding Author:

Allif Rosyidy Hilmi,
Email:
allif_rosyidy.fisika@upnjatim.ac.id

ABSTRACT

This work investigates the optical band gap of polymethyl methacrylate (PMMA) using approaches beyond the conventional Tauc plot. PMMA was prepared via solution casting and analyzed with UV–Vis spectroscopy. Based on the UV–Vis spectra, band-gap values were estimated via the Cody approach, absorption-spectrum fitting (ASF), and a derivative-based ASF variant (DASF), and then benchmarked against the Tauc method. The optical band gap values ranged from 3.10 eV to 4.94 eV, which fall within or near the range reported in the literature for PMMA, depending on the analysis method and transition model used. These values represent effective optical transition energies (apparent optical gaps) of amorphous PMMA rather than true crystalline band-to-band gaps. Each method had distinct advantages: the Cody method provided a clearer linear region for amorphous systems, ASF offered a practical approach that did not require sample-thickness information, and DASF enhanced precision through derivative-based analysis. Band-gap results for both direct and indirect transitions suggest that amorphous PMMA may exhibit more than one effective pathway governing optical transitions. These results show that the Cody, ASF, and DASF techniques can be trusted as effective substitutes for the Tauc method when examining the optical characteristics of polymeric materials.

1. INTRODUCTION

The optical band gap is a key parameter controlling electronic transitions and optical absorption. It represents the minimum photon energy required to promote an electron from the valence band to the conduction band, thereby affecting the material's optical and electronic properties. (Yasin Ahmed, Aziz, & M. A. Dannoun, 2024). In amorphous polymers, the absorption edge can be influenced by disorder-related localized states and the Urbach tail; thus, extracted E_g is interpreted as an effective (apparent) optical transition energy. Precisely determining the optical band gap is crucial for evaluating a material's suitability in various technological fields such as photonics, optoelectronics, and energy devices (Dolgonos, Mason, & Poeppelmeier, 2016).

Polymethyl methacrylate (PMMA) is a transparent thermoplastic polymer characterized by high optical clarity, notable chemical stability, and favorable mechanical

performance (Wu, Ouyang, He, & Huang, 2022). Although PMMA is typically classified as an insulator, understanding its optical band gap is important for applications in polymer-based nanocomposites, coatings, and dielectric layers where light-matter interactions are significant (Abed et al., 2023). A standard approach to estimate the optical band gap is Tauc analysis, which uses a plot of $(\alpha h\nu)^n$ as a function of photon energy; the band-gap value is then extracted by extending the linear segment to its intercept. However, the Tauc method has several limitations, including ambiguity in identifying the linear region, dependence on the assumed transition type, and sensitivity to sub-gap absorption (Dolgonos et al., 2016; Haryński, Olejnik, Grochowska, & Siuzdak, 2022).

To overcome these limitations, several alternative techniques have been proposed, including the Cody method, Absorption Spectrum Fitting (ASF), and Derivative Absorption Spectrum Fitting (DASF). The Cody method extends the Tauc approach by incorporating exponential tail states, making it more suitable for amorphous materials (Makuła, Pacia, & Macyk, 2018). The ASF method uses absorbance data directly, offering a simpler approach that does not require knowledge of sample thickness or absorption coefficients. The DASF method extends the ASF approach by incorporating derivative analysis to enhance precision near the absorption edge (Bhogi et al., 2022).

In this work, PMMA's optical band gap is evaluated using the Cody method, Absorption Spectrum Fitting (ASF), and Derivative Absorption Spectrum Fitting (DASF) as alternatives to the traditional Tauc analysis. By comparing these techniques, we seek to evaluate their reliability, accuracy, and applicability to polymeric systems, and to identify the most effective method for analyzing PMMA's optical properties.

2. METHOD

2.1. Materials and preparation of the sample

The material used in this study was granular poly(methyl methacrylate) (PMMA) obtained from Himedia, India. The granular PMMA was dissolved in acetone at a weight ratio of 1:10. Dissolution was performed under magnetic stirring at 50 °C for 1 h to obtain a fully homogeneous solution. After complete dissolution, the solution was poured into a petri dish maintained at room temperature for 24 hours. This step facilitated gradual solvent evaporation, enabling uniform formation of the PMMA film. The film was characterized by UV–Vis to evaluate optical properties, especially the band gap.

2.2. Determination of optical band gap energy

PMMA's E_g was obtained using Tauc, Cody, ASF, and DASF methods. These techniques are commonly applied to UV-Vis absorption spectra to estimate E_g, each with specific equations and plotting procedures as described below.

2.2.1 Tauc Method

Optical band gaps in amorphous and crystalline semiconductors are often extracted using the Tauc method. It relies on the following equation:

$$(\alpha h\nu)^n = A\left(h\nu - E_g\right)$$

where α is the coefficient of absorption, $h\nu$ is the energy's photon, A is a constant, and E_g is the optical band gap. n depends on the transition: $\frac{1}{2}$(direct) and 2(indirect). To determine E_g, the plot of $(\alpha h\nu)^n$ versus $h\nu$ is extrapolated from the linear section of the curve approaching the x-axis (i.e., where $(\alpha h\nu)^n = 0$). The band-gap energy is then taken from the intercept obtained through this extrapolation (Tauc, Grigorovici, & Vancu, 1966; Ahmed et al., 2024).

2.2.2 Cody Method

The Cody method is often used for amorphous materials that exhibit an exponential absorption tail below the band edge. It modifies the Tauc approach and is defined by the following relation (Raciti et al., 2017):

$$\frac{(\alpha h\nu)}{h\nu} = B\left(h\nu - E_g\right)$$

A plot of $\frac{(\alpha h\nu)}{h\nu}$ versus $h\nu$ yields a straight line near the absorption edge. The linear section of the curve is extended to meet the energy axis, and the intercept defines the Cody optical band gap. This method is considered more accurate for materials with a pronounced Urbach tail because it reduces the influence of sub-gap states.

2.2.3 Absorption Spectrum Fitting (ASF) Method

The ASF method directly uses absorbance A from UV-Vis data and does not require knowledge of sample thickness. The band gap is extracted using the relation:

$$\left(\frac{A}{\lambda}\right)^2 = C\left(\frac{1}{\lambda} - \frac{1}{\lambda_g}\right)$$

where A is the absorbance, λ is the wavelength, C is a constant, and λ_g represents the wavelength associated with the energy's band gap. Plotting $(A/\lambda)^2$ against $1/\lambda$ allows the linear region to be extended until it crosses the x-axis. The intercept at $1/\lambda_g$ is then converted to energy using:

$$E_g = \frac{hc}{\lambda_g}$$

where h denotes Planck's constant and c is the speed of light (Mergen & Arda, 2020; Souri & Shomalian, 2009).

2.2.4 Derivative Absorption Spectrum Fitting (DASF) Method

The DASF method is a refinement of ASF that uses derivative analysis of the absorbance-based function to improve precision near the absorption edge, thereby aiding the evaluation of optical transition behavior. The core equation is:

$$\frac{d}{d(1/\lambda)}\left(\frac{A}{\lambda}\right)^2 \propto \left(\frac{1}{\lambda} - \frac{1}{\lambda_g}\right)$$

The method involves plotting the derivative $\frac{d}{d(1/\lambda)}\left(\frac{A}{\lambda}\right)^2$ against $1/\lambda$, and extrapolating the linear portion to find $1/\lambda_g$. The value of λ_g is then used to calculate E_g, as in the ASF method. This method can enhance edge sharpness and reduce ambiguity in locating the absorption edge, thereby improving the precision of band-gap estimation and supporting comparisons between different transition models (Souri & Tahan, 2015; Bhogi et al., 2022). Before differentiation, spectra were baseline-corrected and smoothed to reduce high-frequency noise that may be amplified by derivative analysis. The derivative was computed numerically on the smoothed data using a consistent step size.

3. RESULTS AND DISCUSSION

Figure 1 shows the UV-Vis absorbance spectrum of PMMA over the wavelength range of 200 to 800 nm. The spectrum exhibits a strong UV absorption feature, particularly below 300 nm, where the absorbance rises sharply and exceeds 4.5 a.u. within the instrument's linear range. This strong UV absorption indicates electronic transitions in PMMA, commonly attributed to transitions involving carbonyl (C=O) groups (e.g., n→π and/or π→π*), consistent with reported optical behavior (Yousefi, Mousavi, Heris, & Naghash-Hamed, 2023). Following the peak, the absorbance rapidly decreases, reaching values near zero around 350 nm. In the

visible to near-infrared region (400–800 nm), the absorbance remains nearly flat and close to zero, indicating that PMMA is highly transparent in this spectral range. Overall, the spectrum exhibits strong UV absorption while remaining highly transparent in the visible range, making it suitable for applications that need UV blocking along with visible light transmission. This spectral behavior enables estimation of the optical band gap using methods such as Tauc, Cody, ASF, and DASF.

Figure 2 presents the Tauc plots for estimating PMMA's optical band gap as a function of energy's photon ($h\nu$) plotted on the x-axis in eV. In Figure 2(a), the y-axis represents $(\alpha h\nu)^2$ $(eV \cdot cm^{-1})^2$, corresponding to an allowed direct transition. In Figure 2(b), the y-axis represents $(\alpha h\nu)^{1/2}$ $(eV \cdot cm^{-1})^{1/2}$, corresponding to an allowed indirect transition. Table 1 shows the optical band gap energies calculated using the Tauc method.

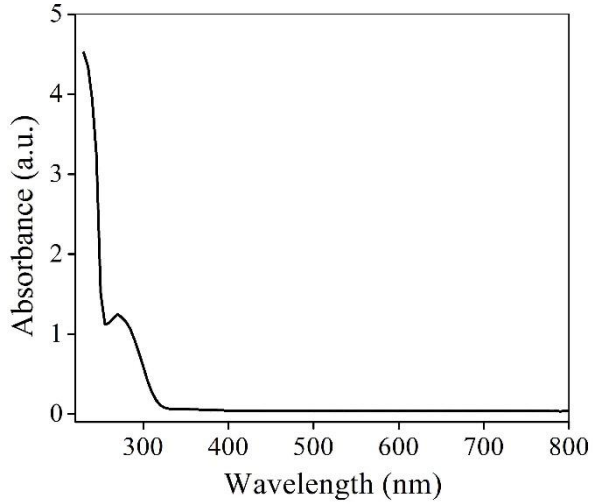

Figure 1. Spectrum of UV-Vis absorbance of PMMA in the range of 200–800 nm.

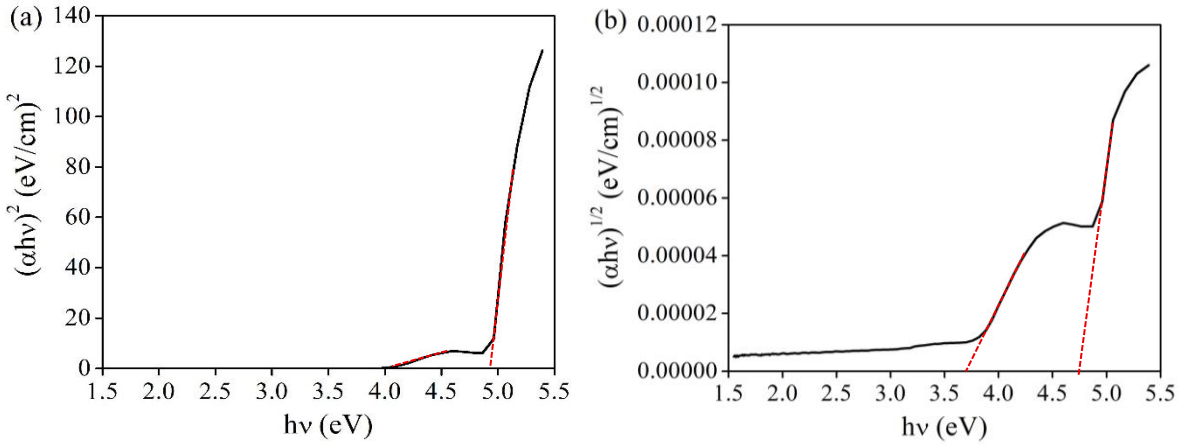

Figure 2. Tauc plots of PMMA for (a) allowed direct transition $(\alpha h\nu)^2$ against $h\nu$, and (b) allowed indirect transition $(\alpha h\nu)^{1/2}$ against $h\nu$. The red dashed lines indicate linear extrapolations used to estimate the optical band gap.

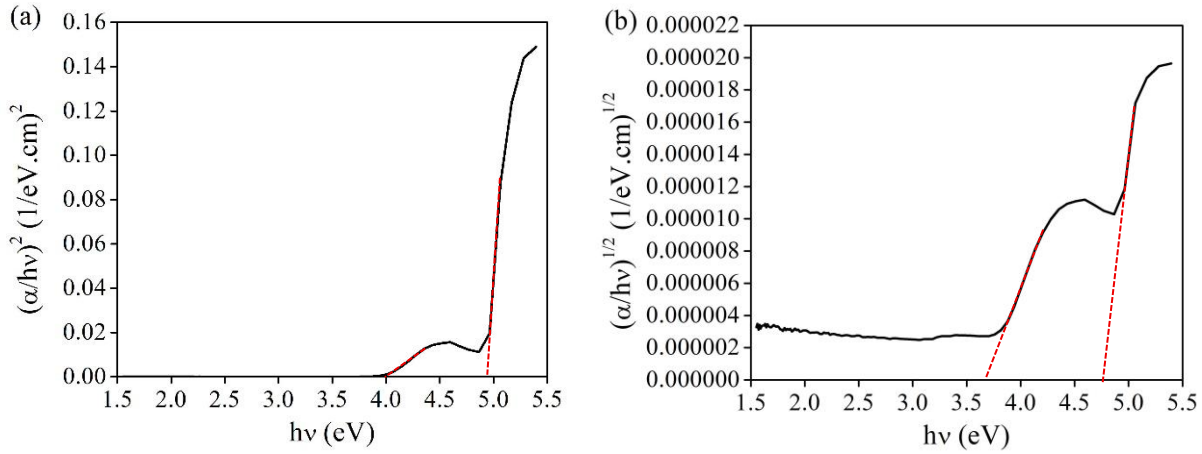

Figure 3. Cody plots of PMMA for (a) direct allowed transition $(\alpha/h\nu)^2$ vs. $h\nu$ and (b) indirect allowed transition $(\alpha/h\nu)^{1/2}$ vs. $h\nu$. Red dashed lines indicate the linear fitting applied to determine the optical band gap energies.

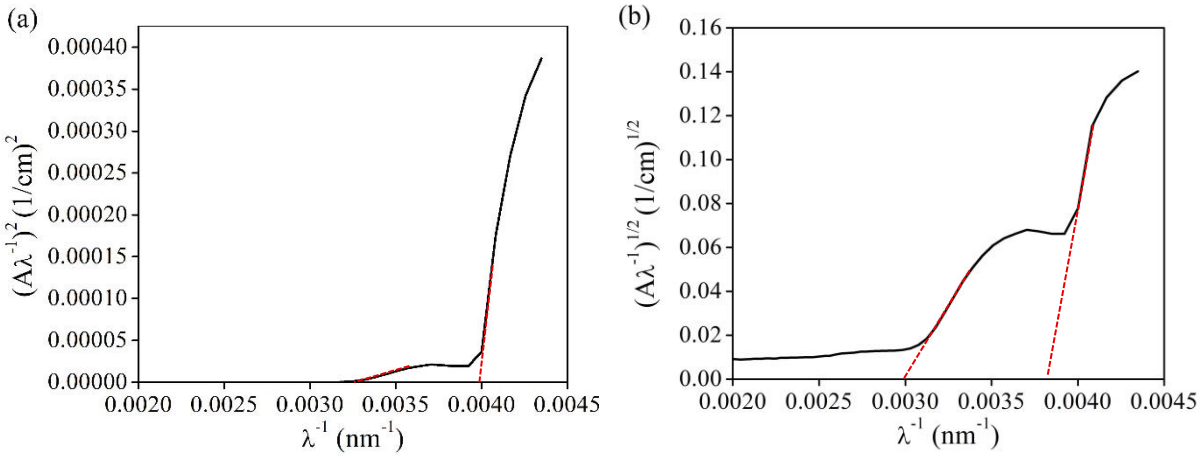

Figure 4. ASF plots of PMMA for (a) direct allowed transition $(A\lambda^{-1})^2$ vs. λ^{-1} and (b) indirect allowed transition $(A\lambda^{-1})^{1/2}$ vs. λ^{-1}. Red dashed lines show the linear fit used to calculate optical band gap energies.

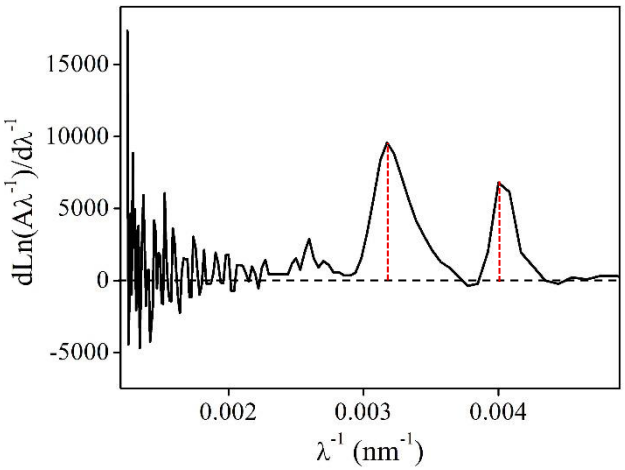

Figure 5. DASF plot of PMMA showing $\frac{d\ln(A\lambda^{-1})}{d\lambda^{-1}}$ as a function of λ^{-1}. The peaks of the curve are used to determine the optical band gap energy of the sample.

Table 1. Optical band gap energies (E_g) of PMMA determined using Tauc, Cody, ASF, and DASF methods for both indirect and direct electronic transitions.

Methods	Transition	E_g (eV)
Tauc	Indirect	4.94; 4.02
	direct	4.78; 3.68
Cody	Indirect	4.94; 4.04
	direct	4.75; 3.68
ASF	Indirect	4.93; 4.04
	direct	4.74; 3.70
DASF		3.91; 3.10

Figure 3 shows the Cody plots used to determine PMMA's optical band gap energies. In Figure 3(a), the y-axis represents $(\alpha/h\nu)^2$ with units of $(1/(eV\cdot cm))^2$, corresponding to the allowed direct transition analysis. Figure 3(b) shows $(\alpha/h\nu)^{1/2}$ with units of $(1/(eV\cdot cm))^{1/2}$, corresponding to the allowed indirect transition analysis. The linear regions of each curve are extrapolated to the photon energy axis (red dashed lines), and the intercepts indicate the estimated optical band gap values for each transition type. The presence of two x-intercepts in panel (b) suggests two distinct linear regions near the absorption edge, which may indicate multiple absorption edges or different effective optical pathways; however, further analysis is needed before attributing them to multiple indirect band gap transitions.

Figure 4 shows the ASF (Absorbance Spectrum Fitting) plots used to estimate the optical band gap energies of PMMA. In Figure 4(a), the vertical axis shows $(A\lambda^{-1})^2$ in units of $(1/\mathrm{cm})^2$ plotted against the inverse wavelength λ^{-1} in nm^{-1}, corresponding to the direct allowed transition analysis. Panel (b) shows $(A\lambda^{-1})^{1/2}$ in units of $(1/\mathrm{cm})^{1/2}$ versus λ^{-1}, representing the indirect allowed transition analysis. The linear portions of each curve, highlighted with red dashed lines, are extrapolated to the horizontal axis, and the intercepts yield the estimated optical band gap values. In panel (b), two linear fits indicate two distinct linear regions near the absorption edge, which may reflect multiple absorption edges or different effective optical pathways; further analysis is required before assigning them to multiple indirect band gap transitions in PMMA.

Figure 5 presents the DASF (Derivative of Absorbance Spectrum Fitting) plot, which is used to identify the optical band-gap energy. The y-axis represents $\frac{d\ln(A\lambda^{-1})}{d\lambda^{-1}}$, while the x-axis is the inverse wavelength $\lambda^{-1}(nm^{-1})$. The peaks in the curve indicate prominent features close to the edge's absorption, related to optical transitions. Peaks were selected based on clear prominence above the local noise floor and their occurrence near the absorption-edge region, while oscillations in the deep-transparent region were excluded. When multiple peaks appeared, the most prominent peak(s) were reported and converted to Eg using the same procedure. These peak positions are then used to calculate the optical band gap energy using the photon energy–wavelength relationship.

As shown in Figures 2 and 3, the key difference between the Tauc and Cody plots for the PMMA sample is the clarity of the linear region before extrapolation. In the Tauc plot, for both direct and indirect transitions, the curve rises sharply only over a limited energy range, producing a shorter linear region. This can make the intercept with the photon energy axis ($h\nu$) less distinct. By contrast, the Cody plots show a more pronounced and extended linear trend near the absorption edge. This facilitates extrapolation and provides a more consistent estimate of the band gap. Overall, these results suggest that the Cody plot offers a more stable

linear representation than the Tauc plot for PMMA, particularly for amorphous absorption edges (Makuła et al., 2018).

As shown in Figures 2 and 4, the differences between the Tauc and ASF analyses for PMMA are small, yielding comparable band gap estimates. Both methods show similar curve profiles and comparable linear fitting regions, resulting in similar band gap estimates. This may be attributed to a well-defined absorption edge in the experimental data, such that differences in the underlying calculation procedures have limited impact on the fitted linear region and the extracted band gap. Moreover, as a transparent polymer, PMMA exhibits an absorption edge in the ultraviolet region, allowing both methods to yield comparable linear representations. Nevertheless, the ASF method offers a practical advantage, as it does not require sample thickness information, making it particularly useful for samples with varying or difficult-to-measure thicknesses.

As shown in Figures 2 and 5, the Tauc plot and the DASF method for PMMA exhibit distinct curve characteristics. In the Tauc plot, the optical band gap is determined by extending the linear portion to intersect with the x-axis of the $(\alpha h\nu)^n$ versus hν plot to the photon energy axis (x-axis), where $(\alpha h\nu)^n = 0$; this linear region often appears at higher photon energies. The selection of this linear region is subjective, depending heavily on the data range chosen by the researcher, which can lead to variations in the results. In contrast, the DASF method analyzes the derivative $\frac{d\ln(A\lambda^{-1})}{d\lambda^{-1}}$ as a function of λ^{-1}, where prominent peaks highlight absorption-edge features that can be used to estimate λ_g (and thus E_g) after appropriate peak selection and conversion. This derivative-based approach produces sharper, more localized spectral features compared to the gradual increase seen in the Tauc plot, enabling a more objective identification of E_g, as the peaks can be determined numerically without excessive visual interpretation. Therefore, DASF can be advantageous when the absorption-edge features are well resolved and the Tauc linear region is ambiguous or limited, potentially improving the consistency of band gap estimation across analyses (Olasanmi et al., 2025).

As shown in Table 1, the optical band gap (E_g) values of PMMA obtained using the Tauc, Cody, ASF, and DASF methods range from 3.10 to 4.94 eV. When compared with the literature, the optical band gap of PMMA is generally reported in the range of 3.1-5.1 eV, depending on factors such as morphology, film thickness, and measurement conditions; thus, the values obtained in this study fall within a reasonable range (Aziz, Abdullah, Hussein, & Ahmed, 2017; Olasanmi et al., 2025; Prasad & Lal, 2022). The appearance of two E_g values for a given transition type (direct or indirect) suggests two distinct linear regions/absorption-edge features in the analyzed spectra. The higher E_g value is often associated with the principal absorption edge, whereas the lower E_g value may reflect sub-band-gap absorption contributions (e.g., tail states/Urbach tail or defect-related states) arising from structural disorder in the polymer. This behavior may be influenced by the amorphous nature of PMMA, which can introduce localized states and lead to multiple absorption-edge features in optical analyses.

Table 2. Comparison of Cody, ASF, and DASF methods in determining the optical band gap, including their equations, curve characteristics, accuracy, and main features.

Aspect	Tauc Plot	Cody Method	ASF Method	DASF Method
Basic equation	Plot $(\alpha h\nu)^n$ vs $h\nu$	Plot $(\alpha/E)^{1/2}$ vs $h\nu$	Plot $(A/\lambda)^2$ or $(A/\lambda)^{1/2}$ vs $1/\lambda$	Plot $\frac{d\ln(A/\lambda)}{d(1/\lambda)}$ vs $1/\lambda$
Curve type	Linear region appears at higher energies; often	Clearer linear region, more stable for amorphous	Relatively long linear region; independent of thickness	Peak-shaped spectrum obtained from the derivative

	affected by initial curvature.			
Accuracy	Moderate to high; strongly depends on the chosen linear region	High, less affected by curvature	High, comparable to Cody	Very high; peaks identified numerically
Advantages	Widely established; simple and standard method	Reduces the influence of curvature; good for amorphous	Does not require thickness information	Objective: minimize subjectivity in extrapolation
Limitations	Subjective choice of linear region; less reliable for amorphous	Still requires linear extrapolation	Sensitive to data quality	Sensitive to noise due to the derivative
Specific features	Best suited for crystalline materials with a sharp absorption edge	Suitable for amorphous materials	Practical for thin films and varying geometries	Superior for consistent comparison across datasets

When determining the optical band gap of PMMA, comparisons among the Cody, ASF, and DASF methods reveal both methodological distinctions and differences in reliability. The Cody approach, which plots functions of α/hν versus photon energy ($h\nu$), is less sensitive to the exponential absorption tail and often yields a more stable linear region for extrapolation. This can improve the consistency of the estimated band gap, particularly for amorphous systems where the linear region in Tauc plots can be ambiguous. Similarly, the ASF method, which uses absorbance–wavelength relations such as $(\frac{A}{\lambda})^2$ or $(\frac{A}{\lambda})^{1/2}$ plotted versus $\frac{1}{\lambda}$, shows good agreement with the Cody analysis for PMMA. The advantage of the ASF method lies in its practicality, as it does not require knowledge of sample thickness, making it suitable for samples with nonuniform geometry. Both methods thus demonstrate comparable accuracy when the absorption edge is well defined, as observed for PMMA (Altalhi et al., 2021; Nawar & El-Mahalawy, 2019).

In contrast, the DASF method applies a derivative-based approach by calculating $\frac{\mathrm{d}\ln(A\lambda^{-1})}{\mathrm{d}(\lambda^{-1})}$ and analyzing the resulting peaks/features near the absorption edge. This procedure can produce sharper and more localized features than the gradual trends observed in Cody or ASF plots, which may reduce ambiguity in identifying the absorption-edge position and the corresponding band gap. The DASF method reduces subjectivity associated with selecting a linear extrapolation region, because the band-gap-related feature can be inferred from peak positions after applying consistent peak-selection criteria. However, derivative processing can amplify experimental noise, requiring careful preprocessing (e.g., smoothing) and consistent data handling. Overall, while Cody and ASF provide robust and practical estimates of E_g, DASF can improve precision by yielding clearer absorption-edge features, which may support more consistent band gap estimation across datasets when preprocessing and peak-selection procedures are standardized (Mamand et al., 2025).

4. CONCLUSION

PMMA band gaps were determined using Tauc, Cody, ASF, and DASF. The estimates were 3.10–4.94 eV, consistent with literature values for PMMA. The results suggest the presence of more than one absorption-edge feature (i.e., multiple apparent/effective band gap values), which may be associated with localized states and structural disorder in amorphous

PMMA. Among the methods applied, Cody and ASF provided practical and consistent estimates, while DASF can improve edge-feature localization and reduce ambiguity when appropriate preprocessing and peak-selection criteria are used. Overall, the findings indicate that Cody, ASF, and DASF can serve as effective alternatives to the conventional Tauc approach for estimating polymer optical band gaps, including that of PMMA.

REFERENCE

Abed, R. N., Zainulabdeen, K., Abdallh, M., Yousif, E., Rashad, A. A., & Jawad, A. H. (2023). The optical properties behavior of modify poly(methyl methacrylate) nanocomposite thin films during solar energy absorption. *Journal of Non-Crystalline Solids*, *609*, 122257. https://doi.org/10.1016/j.jnoncrysol.2023.122257

Ahmed, K. K., Muheddin, D. Q., Mohammed, P. A., Ezat, G. S., Murad, A. R., Ahmed, B. Y., … Aziz, S. B. (2024). A brief review on optical properties of polymer Composites: Insights into Light-Matter interaction from classical to quantum transport point of view. *Results in Physics*, *56*, 107239. https://doi.org/10.1016/j.rinp.2023.107239

Altalhi, T., Gobouri, A. A., Refat, M. S., El-Nahass, M. M., Hassanien, A. M., Atta, A. A., … Kamal, A. M. (2021). Optical spectroscopic studies on poly(methyl methacrylate) doped by charge transfer complex. *Optical Materials*, *117*, 111152. https://doi.org/10.1016/j.optmat.2021.111152

Aziz, S. B., Abdullah, O. Gh., Hussein, A. M., & Ahmed, H. M. (2017). From Insulating PMMA Polymer to Conjugated Double Bond Behavior: Green Chemistry as a Novel Approach to Fabricate Small Band Gap Polymers. *Polymers*, *9*(11), 626. https://doi.org/10.3390/polym9110626

Bhogi, A., Srinivas, B., Padmavathi, P., Venkataramana, K., Ganta, K. K., Shareefuddin, M., & Kistaiah, P. (2022). Absorption spectrum fitting method (ASF), DASF method and structural studies of Li2O–SrO–B2O3–MnO quaternary glass system. *Optical Materials*, *133*, 112911. https://doi.org/10.1016/j.optmat.2022.112911

Dolgonos, A., Mason, T. O., & Poeppelmeier, K. R. (2016). Direct optical band gap measurement in polycrystalline semiconductors: A critical look at the Tauc method. *Journal of Solid State Chemistry*, *240*, 43–48. https://doi.org/10.1016/j.jssc.2016.05.010

Haryński, Ł., Olejnik, A., Grochowska, K., & Siuzdak, K. (2022). A facile method for Tauc exponent and corresponding electronic transitions determination in semiconductors directly from UV–Vis spectroscopy data. *Optical Materials*, *127*, 112205. https://doi.org/10.1016/j.optmat.2022.112205

Makuła, P., Pacia, M., & Macyk, W. (2018). How To Correctly Determine the Band Gap Energy of Modified Semiconductor Photocatalysts Based on UV–Vis Spectra. *The Journal of Physical Chemistry Letters*, *9*(23), 6814–6817. https://doi.org/10.1021/acs.jpclett.8b02892

Mamand, D. M., Muhammad, D. S., Muheddin, D. Q., Abdalkarim, K. A., Tahir, D. A., Muhammad, H. A., … Hassan, J. (2025). Optical band gap modulation in functionalized chitosan biopolymer hybrids using absorption and derivative spectrum fitting methods: A spectroscopic analysis. *Scientific Reports*, *15*(1), 3162. https://doi.org/10.1038/s41598-025-87353-5

Mergen, Ö. B., & Arda, E. (2020). Determination of Optical Band Gap Energies of CS/MWCNT Bio-nanocomposites by Tauc and ASF Methods. *Synthetic Metals*, *269*, 116539. https://doi.org/10.1016/j.synthmet.2020.116539

Nawar, A. M., & El-Mahalawy, A. M. (2019). Simple processed semi-transparent *Schottky* diode based on PMMA-MWCNTs nanocomposite for new generation of optoelectronics. *Synthetic Metals*, *255*, 116102. https://doi.org/10.1016/j.synthmet.2019.116102

Olasanmi, O., Akinsola, S., Yusuf, K., & Aregbesola, E. (2025). Comparative studies for determining the optical band gap energy of CuSe thin films. *Proceedings of the Nigerian Society of Physical Sciences*, 191. https://doi.org/10.61298/pnspsc.2025.2.191

Prasad, S. G., & Lal, C. (2022). Spectroscopic investigations of optical bandgap and search for reaction mechanism chemistry due to γ-Rays irradiated PMMA polymer. *Biointerface Res. Appl. Chem*, *13*(2), 184.

Raciti, R., Bahariqushchi, R., Summonte, C., Aydinli, A., Terrasi, A., & Mirabella, S. (2017). Optical bandgap of semiconductor nanostructures: Methods for experimental data analysis. *Journal of Applied Physics*, *121*(23), 234304. https://doi.org/10.1063/1.4986436

Souri, D., & Shomalian, K. (2009). Band gap determination by absorption spectrum fitting method (ASF) and structural properties of different compositions of (60−*x*) V2O5–40TeO2–*x*Sb2O3 glasses. *Journal of Non-Crystalline Solids*, *355*(31), 1597–1601. https://doi.org/10.1016/j.jnoncrysol.2009.06.003

Souri, D., & Tahan, Z. E. (2015). A new method for the determination of optical band gap and the nature of optical transitions in semiconductors. *Applied Physics B*, *119*(2), 273–279. https://doi.org/10.1007/s00340-015-6053-9

Tauc, J., Grigorovici, R., & Vancu, A. (1966). Optical Properties and Electronic Structure of Amorphous Germanium. *Physica Status Solidi (b)*, *15*(2), 627–637. https://doi.org/10.1002/pssb.19660150224

Wu, W., Ouyang, Q., He, L., & Huang, Q. (2022). Optical and thermal properties of polymethyl methacrylate (PMMA) bearing phenyl and adamantyl substituents. *Colloids and Surfaces A: Physicochemical and Engineering Aspects*, *653*, 130018. https://doi.org/10.1016/j.colsurfa.2022.130018

Yasin Ahmed, T., Aziz, S. B., & M. A. Dannoun, E. (2024). New photocatalytic materials based on alumina with reduced band gap: A DFT approach to study the band structure and optical properties. *Heliyon*, *10*(5), e27029. https://doi.org/10.1016/j.heliyon.2024.e27029

Yousefi, F., Mousavi, S. B., Heris, S. Z., & Naghash-Hamed, S. (2023). UV-shielding properties of a cost-effective hybrid PMMA-based thin film coatings using TiO2 and ZnO nanoparticles: A comprehensive evaluation. *Scientific Reports*, *13*(1), 7116. https://doi.org/10.1038/s41598-023-34120-z